



# AFRL Ludwieg Tube Initial Performance

Roger L. Kimmel\*, Matthew Borg†

*Air Force Research Laboratory, 1950 5th St., WPAFB, OH 45433, USA*

Joseph S. Jewell‡

*NRC Research Associate, Air Force Research Laboratory, 1950 5th St., WPAFB, OH 45433, USA*

King Yiu Lam§

*Spectral Energies, Air Force Research Laboratory, 1950 5th St., WPAFB, OH 45433, USA*

Rodney Bowersox\*\*, Ravi Srinivasan††

*Texas A&M University, College Station, TX*

Steven Fuchs††, Thomas Mooney§§

*University of Dayton Research Institute, Dayton, OH*

The Air Force Research Laboratory has developed and constructed a Ludwieg tube wind tunnel for hypersonic experimental research. This wind tunnel is now operational and its initial performance has been characterized. The tunnel is configured with a 30 inch diameter, Mach 6 nozzle. It is designed to operate with diaphragm or valve actuation. The wind tunnel provides 0.2 seconds of Mach 6 flow during each run. Each run consists of two periods of steady flow at different Reynolds numbers, each of which is approximately 0.1 second in duration. Pitot pressure measurements and schlieren images show good flow uniformity. Pitot pressure fluctuations are approximately 2.5% with a clean diaphragm break, and about 3% using a fast valve. Tests using Mylar®, aluminum and steel diaphragms have shown a correlation between the quality of diaphragm breakage and Pitot pressure fluctuations.

## I. Introduction and Background

Ludwieg tube type wind tunnels have become popular tools for basic research due to the simplicity of their design and the minimal infrastructure required to support them. The Aerospace Systems Directorate of the Air Force Research Laboratory in Dayton, OH, has constructed a hypersonic Ludwieg tube for bench level scientific and technical research. The mission of this wind tunnel is to provide hands-on access for engineers to conduct basic research in fluid dynamics, instrumentation development and related disciplines. This paper describes the design and performance characteristics of this new wind tunnel.

The operating principle of the Ludwieg tube has been described in numerous publications (for example, Friehmelt et al. <sup>1</sup>). In summary, Ludwieg tube tunnels consist of a high-pressure end (storage or driver tube) that acts as a stagnation chamber, and a low-pressure end (nozzle, test section and vacuum tank, if so equipped). An actuation device such as a diaphragm or fast valve isolates the high- and low-pressure legs of the system. When the tunnel is actuated, an expansion wave train moves upstream in the driver tube. If the actuation time is sufficiently short, a period of time exists when conditions are constant after the passage of the expansion wave, providing a period of steady stagnation conditions until the wave train reflects from the most upstream end of the driver tube and returns to

\* Principal Aerospace Engineer, Associate Fellow AIAA

† Aerospace Engineer, Senior Member, AIAA

‡ Research Associate, Senior Member, AIAA

§ Engineer, Member, AIAA

\*\* Professor, Ford I Professor and Department Head, Associate Fellow AIAA

†† Research Associate, Member AIAA

‡‡ Distinguished Research Engineer

§§ Research Engineer

the region of the nozzle contraction. If the stagnation pressure after the first expansion wave passage is sufficiently high, one or more additional periods of uniform flow may succeed the initial test period.

Several Ludwieg tubes with fast-opening valves have been constructed. These include wind tunnels at Technical University Braunschweig,<sup>2</sup> University of Delft,<sup>3</sup> King Abdul-Aziz University<sup>4</sup> and the AF Academy<sup>5</sup>.

## II. Design Features

The AFRL Ludwieg tube was designed to provide as much operating flexibility as possible. Figure 1 presents a rendering of the assembled tunnel. The operating design point is Mach 6, and the tunnel currently operates at this condition. However, two additional nozzles for Mach 4 and 8 were designed, and the system is sized to accommodate them. The primary method of actuation is a fast valve, but the tunnel was also designed to accommodate diaphragm actuation. The driver tube contains numerous access points for diagnostics. The diffuser and vacuum tanks also contain access ports. The test section contains windows on three sides and an autoclave door for quick access. This section describes the wind tunnel on a component-by-component basis.

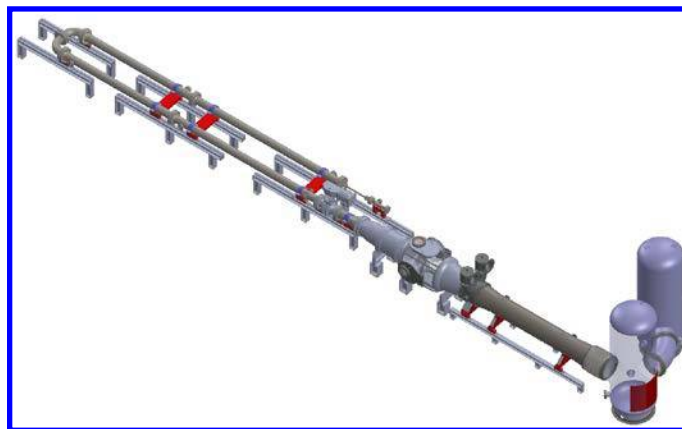


**Figure 1** Perspective rendering of Ludwieg tube

The tunnel is powered by two compressors and two vacuum pumps to provide redundancy in case of maintenance or repairs. Compressors are Sauer 580 psi, 50 SCFM models, operating at 27 HP each. The vacuum pumps are Leybold 444 CFM models, operating at 25 HP each. The compressors and vacuum pumps were sized to accommodate a five-minute turnaround time when operating at a stagnation pressure of 220 psia (freestream unit Reynolds of  $4 \times 10^6/\text{ft}$  and Reynolds number based on nozzle diameter of  $10^7$ ). At the upper limit of stagnation pressure (580 psia), the tunnel unit Reynolds number is  $10.5 \times 10^6/\text{ft}$  ( $\text{ReD} = 26 \times 10^6$ ), with a pumping time of about 12 minutes.

Filling and purging of the driver tube is accomplished through 1 inch and 2 inch diameter schedule 40 stainless steel lines, respectively. A valve assembly consisting of three 2 inch ball-valves controls the fill and purge process. A commercial Sylvania 18 kW resistance heater raises the inlet air temperature to 500K prior to filling the driver tube. The Ludwieg tube does not use an accumulator tank. Instead, the compressors run continuously during operation. After the driver tube is charged to the desired pressure, a bypass valve opens, dumping compressed air outside. This scheme eliminates the need for accumulator tanks, assures that the maximum pressure in the system is no higher than the driver tube rating, and minimizes compressor starting and stopping.

The driver tube consists of 9.75 inch ID, 304 stainless steel. Two 20 ft and two 15 ft sections comprise the driver tube. The driver tube is assembled in two parallel legs joined by two 90° elbows, forming a 180° U-bend. This 180° reflexed driver tube configuration has been used previously on several Ludwieg tubes.<sup>1, 2, 3</sup> Unsteady CFD (Section III) confirmed that the U-bend would not generate undesirable wave reflections. The driver tube air used during the first two 100 ms test periods originates from the first 30 feet of the driver tube nearest the nozzle, so this flow has not passed through the U-bend and been contaminated by secondary flow. The driver tube is mounted on wheeled carriages on a rail so that it can be rolled back and forth as necessary to access components and to accommodate thermal expansion.

The driver tube was hydrostatically tested and code-stamped. The driver tube contains eight 3 inch diameter instrumentation ports capped by blind flanges. These ports permit instrumentation to be introduced into the driver tube via the blind flanges. The flanges may be drilled to accommodate instrumentation without compromising the driver tube code stamp. The total internal length of the driver tube is 82 feet. This length provides approximately 100

ms of uniform run conditions between wave passages. The exterior of the driver tube is heated with blanket resistance heaters to 500 K to minimize thermal losses from the driver air to the tube walls. Unlike some Ludwieg tubes (for example Refs. 1, 2) the entire length of the driver tube is heated to avoid convection and driver tube diameter changes required for non-uniform heating.

The tunnel nozzle was assembled in three sections consisting of a 316 stainless steel throat and two 6061-T6 aluminum downstream sections. The sections were rough-forged to shape, then machined to final contour. The nozzle was designed using method of characteristics, and the contour was verified using Reynolds averaged viscous computational fluid dynamics (GASP by Aerosoft, Inc); more details are given in Section III.A. Viscous corrections to compensate for boundary layer growth on the nozzle wall resulted in a 23% larger area ratio than the inviscid one required for Mach 6. The nozzle throat is 3.71 inches in diameter, and its exit is 30 inches diameter. A ten-inch length upstream of the nozzle throat contains a 10 inch diameter straight lead-in, followed by the contraction. The entire nozzle assembly is 117 inches long.

The nozzle terminates in a test chamber approximately 50 inches in diameter and constructed of carbon steel. The test chamber contains three circular hatches, one on the top and one each on the west and east faces of the test chamber. The east hatch is an autoclave door that provides rapid access to the test section. Both east and west hatches contain 12 inch diameter windows, currently containing fused silica transparencies. The top contains a 4 inch diameter calcium fluoride window for infrared measurements.

The downstream portion of the test chamber contains a capture cone of 44 inch diameter that channels flow into the diffuser. The diffuser consists of a straight pipe, 127 inches long and 29.5 inches ID. The inlet to the diffuser is 6-deg converging cone, and the exit is a 4-deg diverging cone. The tunnel includes a safety vent section between the test chamber and the inlet to the diffuser. The safety vent consists of two 12 inch flapper valves set to open at an internal pressure just above atmospheric. The 12 inch valves connect via a Y-shaped junction to a 22 inch exhaust duct that conducts air outside the tunnel building.

A 30 inch diameter flex coupling connects the downstream end of the diffuser to a double receiver tank. The tunnel design originally called for one 3800 gallon ( $508 \text{ ft}^3$ ,  $14.4 \text{ m}^3$ ) receiver tank. In order to conform to the room dimensions, the single tank was replaced with two 2000 gallon tanks connected with an elbow joint. Six inch diameter schedule 40 stainless steel pipe connects the vacuum tanks to the vacuum pumps on the lower level of the building. The tank immediately downstream of the diffuser contains a removable internal doubler to absorb any inadvertent debris impacts without damaging the main wall of the tank.

The Ludwieg tube was designed to accommodate either a large ball valve, diaphragms, or a plug-type fast valve for actuation. The ball valve is a 10 inch diameter, full bore design. It is pneumatically actuated, with an opening time of 1.1 seconds. Although this valve requires multiple driver tube wave passage cycles to fully open, the utility of an off-the-shelf valve outweighed the drawbacks of the relatively long opening period. The diaphragm capability was added to mitigate risk from valve performance. Unlike some fast valve Ludwieg tubes, the AFRL Ludwieg tube has no requirement for a fast-closing valve. The driver tube is simply recharged from its end-of-run equilibrium pressure each time.

The tunnel is operated via Ethernet using a programmable logic controller. Compressor and vacuum pumps may be remotely started and stopped from the control room using this system. The tunnel is also charged, discharged and fired using the same system. Tunnel process data are acquired using a Gantner data acquisition system (16 channels, 24-bit,  $10^5$  samples/s plus additional thermocouple channels). Measurement data are acquired using an HBM Genesis system (48 channels, 18 bit, 2MS/s plus 8 channels of 14 bit,  $10^8$  samples/s) for higher bandwidth instrumentation. Wind tunnel pressure transducers are calibrated using a Mensor precision pressure reference. Since the test section may be isolated and evacuated prior to test, pressure sensors may be easily gang-calibrated in situ at any time, which greatly improves the precision of pressure measurements.

### III. Design and Analysis

#### A. Conceptual and Preliminary Design and CFD

The tunnel design process started with a 1D inviscid, perfect gas analysis to size components. The target conditions were freestream Mach 6 and minimum run time of 100 msec. The conceptual design process considered four options. These configurations consisted of 30 inch nozzles with 10 inch and 16 inch diameter driver tubes, and 20 inch diameter nozzles with 10 inch and 6 inch driver tubes. The 30 inch nozzle with a 10 inch driver tube was selected for more detailed analysis since it provided maximum size within budget. The Mach 6 flow requirement enforced a stagnation temperature of 500 K to avoid air liquefaction in the test section. The wave passage time in the driver tube is given approximately by

$$t \approx 2L/a$$

With sound speed,  $a$ , determined by the stagnation temperature, and a requirement for a wave passage cycle minimum time of 100 msec, this determined the minimum driver tube length,  $L > 75.5$  ft (23.0 m).

Although the design point for the wind tunnel was M=6, M=4 and 8 nozzles were also designed, but not built. This was done to ensure that the tunnel footprint could accommodate these nozzles to expand the device Mach number range in the future. A method of characteristics (MOC) code was used to design the nozzles. Limited steady and unsteady CFD analysis demonstrated Mach 6 nozzle and driver tube performance. CFD analysis utilized the GASP CFD code. A 2D structured axisymmetric grid was used in the GASP nozzle analysis. Cubic splines were fit to the MOC wall points, and the resulting curves were used to generate the CFD grids. The inlet of the domain, i.e. the inlet of the subsonic section, was located 10 inch (25 cm) upstream of the throat. Total pressure and temperature values were used at the inlet. Axisymmetric conditions were used at the axis of the nozzle and viscous wall conditions were used at the nozzle surface. The initial exit boundary condition used was a low back pressure to ensure that the nozzle was started. The boundary condition was then changed to extrapolation as the flow became supersonic in the diverging section. Inviscid fluxes are evaluated using the 3rd order MUSCL formulation, and 2nd order accurate reconstruction was used for viscous terms. Menter's SST was used as the turbulence model in this simulation. Fine and medium grid calculations showed that the analysis was spatially resolved. The fine grid had 276260 points (149 points in the wall normal direction) and the medium had 69764 points (75 points in the wall normal direction). Figure 2 illustrates the results of the nozzle CFD simulation. These data show that the results are grid independent, that the exit Mach Number was uniform to with 1.5% across the nozzle exit, with a nozzle wall boundary layer approximately 2.4 inch (6 cm) thick.

The inviscid throat diameter for a Mach 6 nozzle with a 30 inch diameter exit is 4.114 inches (104.5 mm). Since the exit diameter is effectively decreased due to boundary layer growth on the nozzle wall, the nozzle throat diameter was also decreased accordingly, to 3.71 inches (94.2 mm), to maintain a Mach number of six at the nozzle exit. The area ratio between the throat and driver tube determines the driver tube Mach number, approximately 0.08 in the absence of viscous effects. CFD using GASP (Figure 2) showed a very uniform Mach number distribution across the nozzle exit, with a nozzle wall boundary layer approximately 6 cm thick.

A time-dependent simulation of the nozzle and driver demonstrated that the device would produce steady flow, with no adverse effects from the U-bend in the driver tube. A 3D grid was used for the unsteady simulations. The unsteady calculations utilized a grid density equal to the medium grid used in the 2D simulations. The grid utilized a symmetry surface (along the XY plane) to reduce simulation time. The grid for the simulation is shown in Figure 3 (every other point is shown for clarity). The unsteady flow equations were solved using a dual-stepping method with 2nd order accuracy in time. Other simulation parameters were similar to those used in the 2D nozzle simulations. The simulations required multiple submits due to a limitation of 140 wall clock hours per job. A 140 wall clock hour job with 128 CPUs (that is, 17920 CPU hours) simulated about 10 msec of tunnel operation at the initial time step. Time step ramping was used to speed up convergence, where ultimately four submits were required.

Figure 3 shows the total pressure time trace, which demonstrated that the total pressure would be time invariant for the proposed geometry for nominally 100 msec. Tunnel start was assumed to be impulsive, similar to an ideal diaphragm breakage. The data also showed the expected total pressure for the second passage of the unsteady expansion. Figure 3 also shows contour and line plots of the propagation of the expansion and nozzle exit flow.

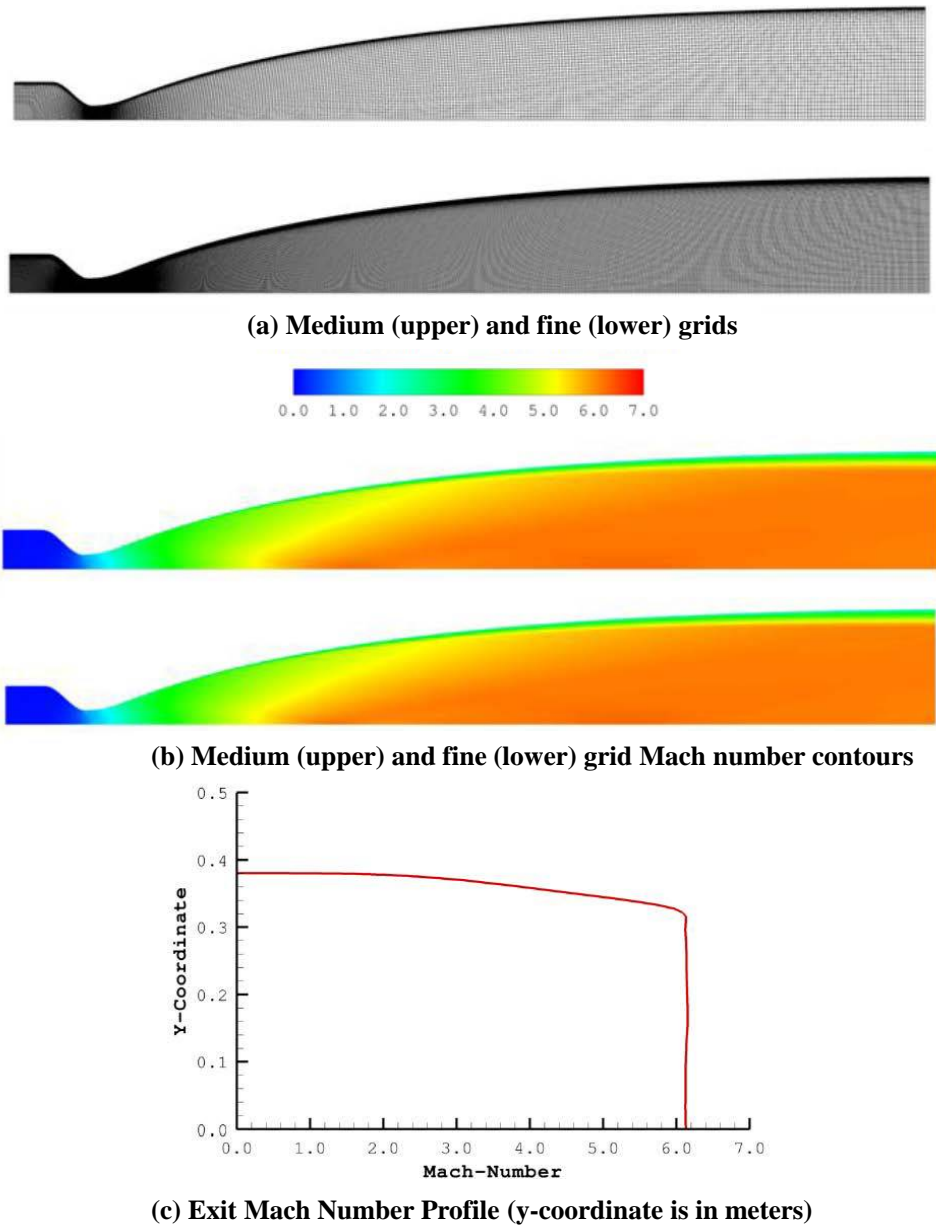
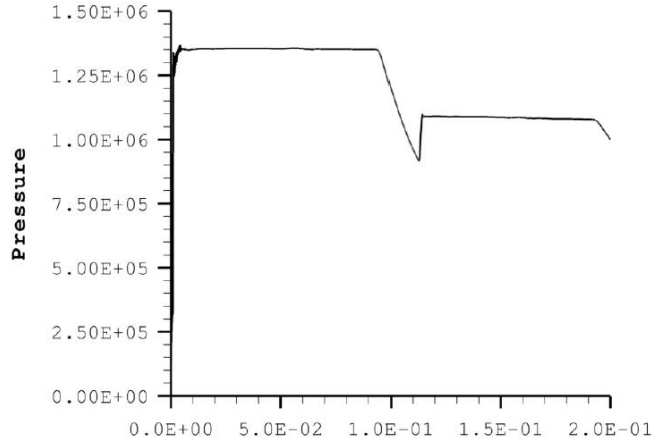


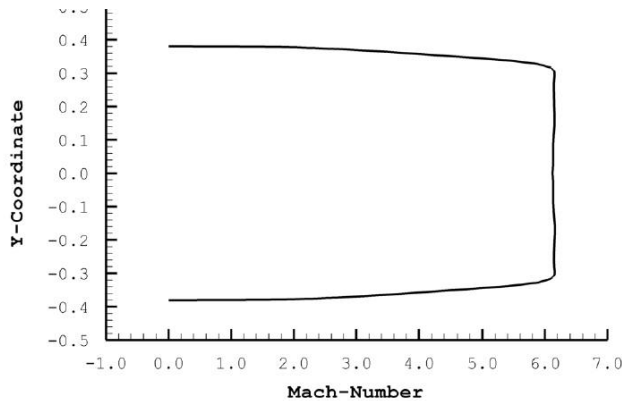
Figure 2 M=6 nozzle CFD results



**(a) Time trace of total pressure upstream of the nozzle (pressure in Pa, time in seconds)**



**(b) Pressure contour early in the tunnel run**



**(c) Nozzle exit Mach number profile**

**Figure 3 Unsteady simulation results**

## B. Detailed Design and Construction

During the detailed design phase, a number of modifications were made to ease fabrication, lower cost and improve operability. During the detailed design phase, finite-element analysis was conducted to size components and ensure appropriate factors of safety.

During detailed design, additional modifications improved manufacturability and operability. Most notably, the test section and diffuser design were changed from rectangular to circular cross sections. This design change alleviated sealing issues between sidewalls and the top and bottom, and improved the structural soundness of the design. The use of standard pipes or rolled and welded stock also reduced the required machining operations. In addition to this change, the single vacuum receiver tank was replaced by two tanks. Also, the driver tube was rotated 90 deg to move

the plane containing the two legs of the driver tube from a vertical to a horizontal orientation. This move simplified support and alignment of the reflexed leg of the driver.

The decision was made early in conceptual design to place the starting actuator upstream of the test section, rather than downstream of the test section. The advantage of placing actuation downstream of the test section is that if diaphragms are used, any debris from a poor diaphragm rupture would not damage the nozzle or test section. The drawback of this design is that the entire test section must be pressurized to the driver tube initial pressure. This results in a heavy and more costly test section, generally with poorer visual and physical access. Upstream actuation obviates these concerns, but brings different risks from diaphragm debris or impaired flow quality due to valve wakes.

The downstream portion of the Ludwieg tube was rated to withstand at least 58 psia internal pressure, based on worst-case failure scenarios. As an added safety measure, vents were added to the downstream section. This requirement resulted in the addition of the two 12 inch diameter relief valves. These valves were specified to open at slightly above atmospheric pressure. Under normal operation, the valves will remain closed at all times during operation when driver pressures are below about 400 psia. Operation at stagnation pressures above 400 psi will result in super-atmospheric pressure in the test section, producing some venting through the relief valves.

#### IV. Performance

##### C. Test Procedures

Figure 4 shows the location of pressure sensors in the Ludwieg tube. During diaphragm actuation, the tunnel was operated at stagnation pressures of 50 to 300 psia. During fast-valve tests, the tunnel was operated at stagnation pressures ranging from 100 to 580 psia. A rake was also installed in the test section to monitor Pitot pressure. The size of the rake was minimized to prevent blockage and avoid loading on the support sting during tunnel start and unstart. Kulite® transducers were placed 1.75 and 5 inches to each side of the sting centerline. The rake was a probeless configuration<sup>6</sup> to accommodate available large diameter transducers (Kulite® XTEL-190) without unreasonably-sized probes, and to provide a mechanically strong device. One lower-range Kulite® was installed in a probe configuration to compare to the probeless transducers.

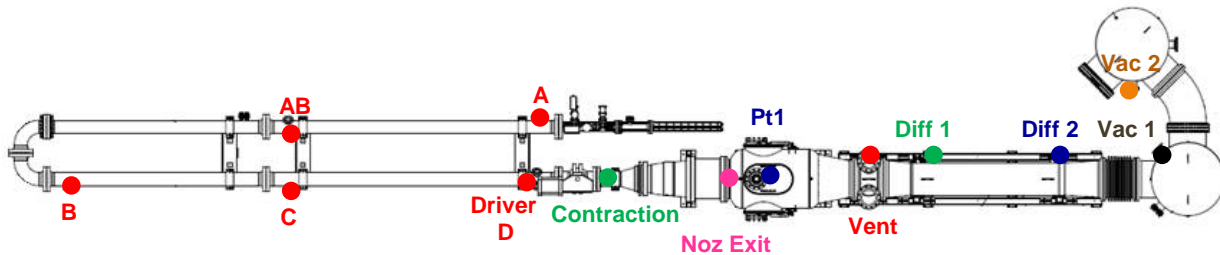


Figure 4 Ludwieg Tube pressure sensor locations

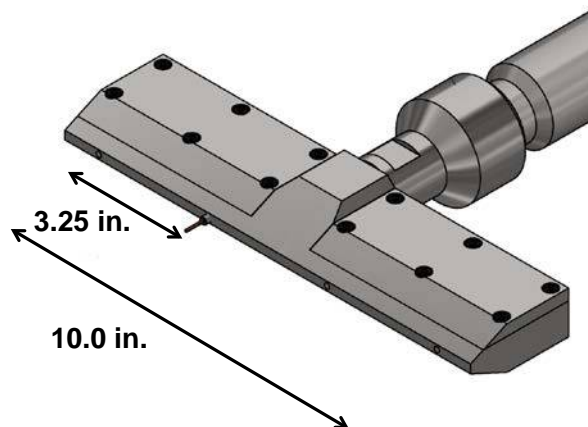


Figure 5 Pitot rake

#### D. Fast-Valve Actuation and Test Conditions

A plug-type fast-opening valve was acquired and tested. This valve is the same design used in multiple wind tunnels in Europe and the US.<sup>1, 2, 7</sup> The benefit of this valve is that it opens rapidly (less than 50 ms), and can be cycled for another run within the time required to evacuate the downstream end of the Ludwieg tube and pressurize the driver tube. The centerbody of the valve and its supports create a flow obstruction in the driver tube. Although wakes from the valve body may compromise test section flow uniformity and noise characteristics, this has not been a major problem with wind tunnels using this type of valve. However, there has been no direct comparison of flowfields from this valve and those from a fully-open diaphragm. The dual actuation capability of the AFRL Ludwieg tube presented an opportunity to conduct this comparison.

One complication of the Ludwieg tube is that the test gas reservoir conditions are not equal to the pre-run driver tube conditions, but are instead equal to conditions behind the expansion wave. Driver tube pressure may be monitored, but it is difficult to measure driver tube temperature with adequate frequency response. Because of this, it is useful to have predicted post-expansion driver tube conditions to compare to measurements. Although the driver tube superficially resembles a shock tube, the driver tube flow is somewhat more complex since it must accommodate the nozzle boundary conditions at the downstream end of the driver tube. The method used here, described by Knauss et al.<sup>8</sup>, is applicable to fast-valve actuation. It requires that the driver tube post-expansion Mach number satisfies continuity throughout the downstream portion of the nozzle. This post-expansion Mach number determines the strength of the expansion wave, from which other properties follow. The driver tube Mach number is determined from the driver tube and throat areas via conservation of mass, assuming isentropic flow,

$$\left(\frac{A_{DT}}{A^*}\right)^2 = \frac{1}{M_{DT}^2} \left[ \frac{2}{\gamma+1} \left(1 + \frac{\gamma-1}{2}\right) M_{DT}^2 \right]^{(\gamma+1)/(\gamma-1)} \quad (1)$$

The driver tube drift velocity following an expansion wave is related to the pre- and post-expansion sound speeds by<sup>9</sup>

$$u_{DT} = \frac{2}{\gamma-1} (a_i - a_{DT}) \quad (2)$$

Equation (2) may be expressed in terms of Mach number and temperature using relations for isentropic flow and sound speed

$$\frac{T_i}{T_{DT}} = \left(1 + \frac{\gamma-1}{2} M_{DT}\right)^2 \quad (3)$$

Finally, knowing the driver tube post-expansion static temperature and Mach number, the driver tube post-expansion stagnation temperature may then be obtained, using the isentropic relation

$$\frac{T_0}{T_{DT}} = 1 + \frac{\gamma-1}{2} M_{DT}^2 \quad (4)$$

The ratio of post-expansion driver tube stagnation temperature to initial driver tube temperature is then obtained from equations (3) and (4)

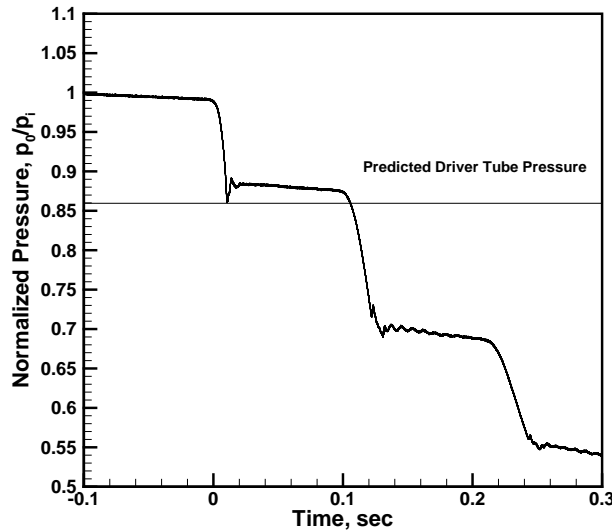
$$\frac{T_0}{T_i} = \frac{1 + \frac{\gamma-1}{2} M_{DT}^2}{\left(1 + \frac{\gamma-1}{2} M_{DT}\right)^2} \quad (5)$$

Again, assuming isentropic flow, post-expansion stagnation pressure and density are obtained from equation (5)

$$\frac{p_0}{p_i} = \left(\frac{\rho_0}{\rho_i}\right)^\gamma = \left(\frac{T_0}{T_i}\right)^{\gamma/(\gamma-1)} \quad (6)$$

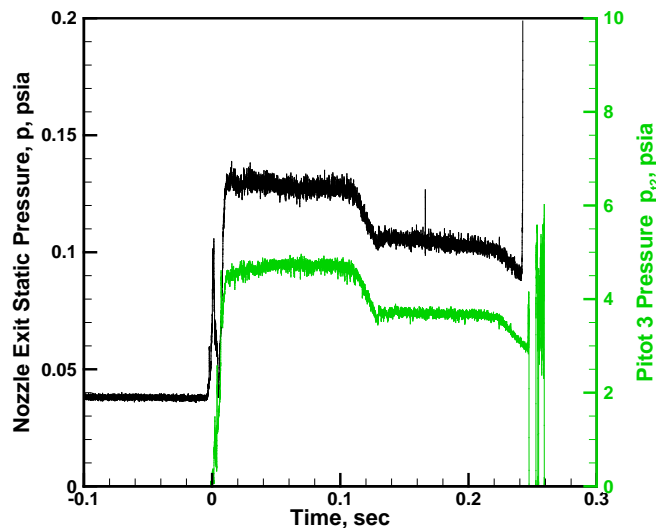
For the AFRL Ludwieg tube, the above analysis predicts temperature and pressure ratios are  $T_0/T_i=0.97$ , and  $p_0/p_i=0.89$ . The expected driver tube Mach number, based on the driver tube inside diameter and nozzle throat diameter, is 0.084, neglecting viscous effects. Due to the low driver tube Mach number, the post-expansion driver tube static temperature and pressure are within 0.5% of stagnation conditions.

Figure 6 illustrates pressure measured in the driver tube at location D during a fast-valve run. For presentation purposes, the data plotted in Figure 6 were digitally notch-filtered between 500-2000 Hz to remove a ringing that arose from a cavity in front of the sensor due to its installation, and low-pass filtered below 20 kHz to remove electronic noise. For Pitot noise analysis shown later in the paper, these filters were not applied. Initial pressure for this run was 208 psia. Several features of this graph are notable. First, the valve opened within about 20 ms, based on examination of the pressure signal. The total time between valve-opening and the first expansion wave reflection was 100 ms, as expected. About 80 ms of quasi-steady pressure was obtained after the valve-opening transient. Pressure during this time was reasonably flat, with a droop of about 0.2%. The isentropic wave analysis described above predicted the run pressure within the transducer accuracy.



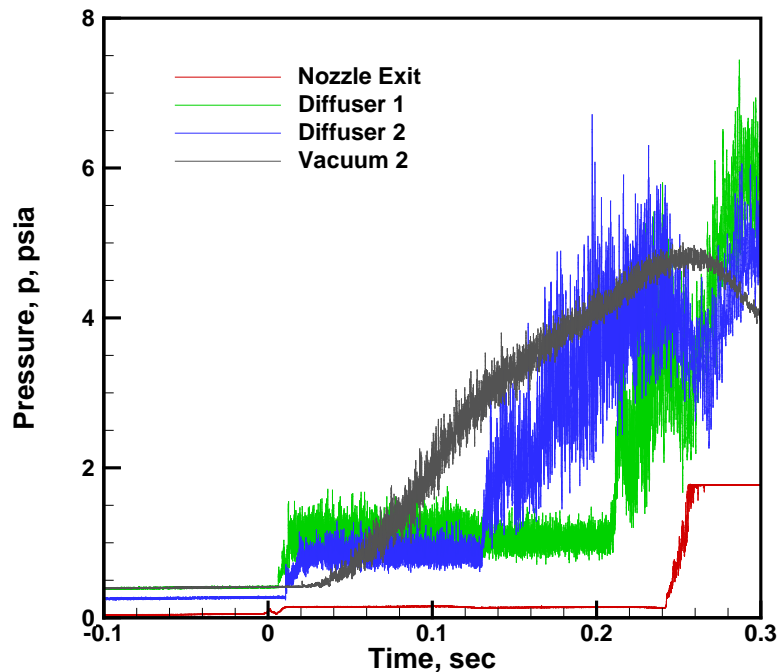
**Figure 6** Driver tube pressure during fast-valve run, transducer D

Figure 7 illustrates the nozzle exit static pressure and Pitot pressure (Pitot 3) measured during the same run. The initial starting shock is visible near  $t=0$ , followed by two periods of quasi-steady flow of about 100 ms each, separated by an expansion-wave passage. During the passage of the second expansion wave (at about  $t=0.22$  s), the tunnel unstarted.



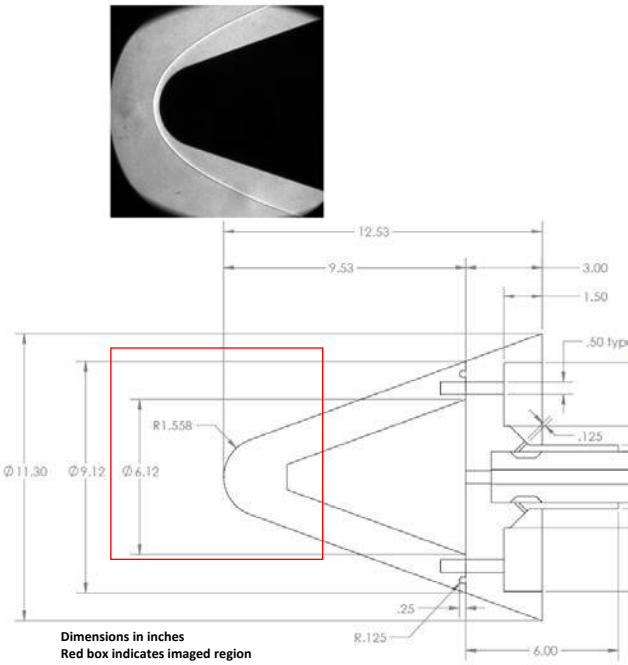
**Figure 7** Nozzle and Pitot pressures during fast-valve run

Figure 8 illustrates the tunnel unstart process and diffuser performance. These pressure traces show an orderly progression through the unstart process. Receiver tank vacuum pressure began to rise about 20 ms after tunnel start. Although the receiver pressure rose continuously through the run, diffuser pressures remained steady for the first 120 ms of the run. After the first reflected expansion wave passage, the downstream diffuser pressure began to rise, eventually approaching the receiver tank pressure, indicating the beginning of unstart in the diffuser. Although the downstream portion of the diffuser had unstarted, the upstream portion of the diffuser and the nozzle remained started. After the second wave passage at about  $t=210$  ms, the upstream portion of the diffuser unstarted. About 30 ms later, this unstart wave structure had transited upstream through the test section and had reached the nozzle exit. By the time this point in the unstart process occurred, the receiver tank pressure was nearly equal to the test section Pitot pressure, 4.8 psia, indicating satisfactory diffuser performance.



**Figure 8 Unstart process during fast-valve operation**

A polymer blockage cone was tested to assess the tunnel's ability to accommodate large models. This model was tested using the fast valve at a variety of stagnation pressures from the tunnel maximum of 580 psia to the lowest pressure at which the fast valve would operate, 114 psia. Figure 9 shows a dimensioned sketch of the blockage model. The model consisted of a 22 deg half-angle blunt cone, with a nose radius of 1.558" and a base diameter of 11.3 inches. Figure 9 also shows a schlieren image of the first several inches of the cone, illustrating a clean, steady bow shock, demonstrating that the tunnel had started. This model started at all stagnation pressures tested. Pressures measured in the diffuser and nozzle also indicated steady Mach 6 flow for all conditions tested.



**Figure 9 Blunt cone model sketch and schlieren image.**

### E. Diaphragm Actuation

Diaphragm actuation of the Ludwieg tube provided a means to accomplish a true impulsive tunnel start, and provided a baseline to which valve actuation could be compared. Both metal and Mylar® diaphragms were tested. Mylar® diaphragms were ruptured using a melt wire technique. Generally, the melt wire did not result in complete diaphragm breaks, and the technique requires additional development. Aluminum and steel diaphragms were tested in double-diaphragm and single-diaphragm configurations. Best results, in terms of clean diaphragm breaks, were achieved with the single-diaphragm runs. In these tests, single metal diaphragms were pre-scored and ruptured simply by increasing tunnel pressure. However, comparison of incomplete to clean diaphragm breaks provided data on the influence of upstream obstructions on wind tunnel noise. Continued refinement of the double-diaphragm and melt-wire designs are required to achieve more reliable diaphragm breakage.

The assumption of isentropic flow applied to the fast valve is also applicable to diaphragm actuation. A concern with the AFRL Ludwieg tube is the shock that occurs when the tunnel is actuated with a diaphragm. Since the diaphragm is upstream of the nozzle, the shock from the diaphragm rupture partially reflects from the converging section of the nozzle. Upstream of the diaphragm location, driver tube pressures initially drop below their equilibrium values as the expansion wave passes, then recover to equilibrium after the passage of the shock reflected from the contraction. The reflected shock is three-dimensional and relatively weak however, so that this expansion and recompression process is largely isentropic. Driver tube pressure during fast-valve and single diaphragm actuation are compared in Figure 10. Driver tube pressure in this figure was normalized by pre-run pressure. The normalized pressures during the diaphragm-actuated run were similar to the fast-valve actuated run. The starting transient for the diaphragm was shorter, compared to the fast valve. In both runs, the tunnel unstarted approximately 200 ms after actuation, producing two 100 ms-long periods of quasi-steady flow.

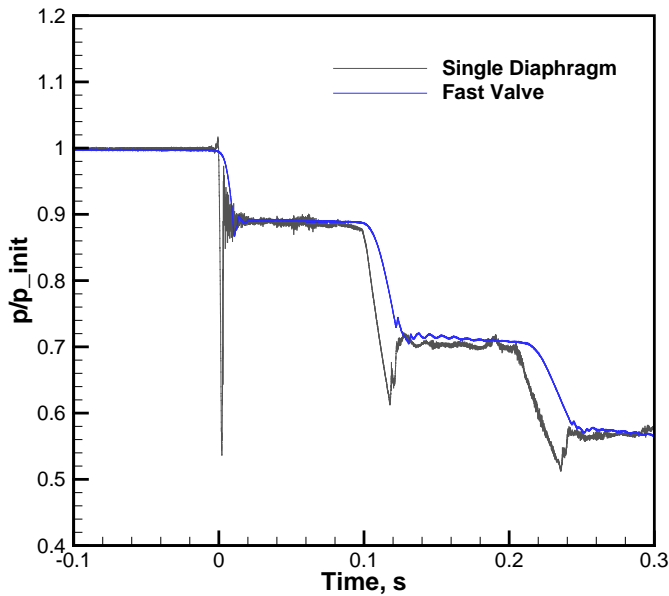


**Figure 10** Driver tube transducer D pressures during fast valve and single diaphragm actuation.

The driver tube wall was maintained at 500 K at all times. Although the driver tube was instrumented with thermocouples on its inner surface, these thermocouples were not recorded during initial testing. Since the driver tube gas temperature was not measured directly, a secondary method based on wave arrival times was used to estimate the driver tube initial gas temperature. Knowing the location between pressure sensors and the time delay between the arrival of the leading expansion wave, the sound speed and hence temperature could be determined. Figure 11 shows an example of this arrival time analysis. Actuation for this case was a single diaphragm, which provided a sharply defined expansion wave. The slope of a linear curve fit of distance versus arrival time indicated a sound speed for this case of 442 m/s, equating to a driver tube stagnation temperature of  $T_i=486$  K, 5% lower than the wall temperature measured with wall thermocouples. Although this method was not analyzed in more detail, it may provide an alternative to thermocouples for driver tube temperature measurement.

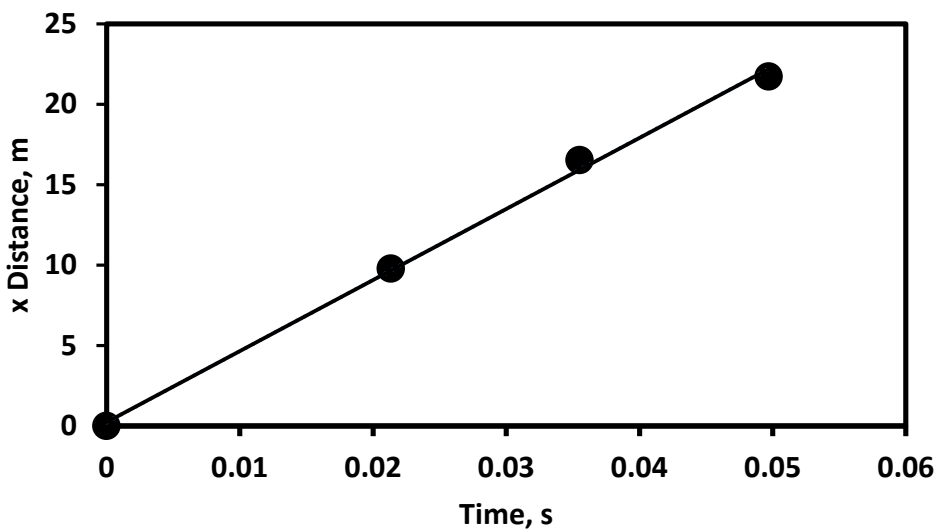


**Figure 11** Expansion wave arrival times

Residual turbulence in the driver tube from the filling process has been posited as a potential noise mechanism in quiet Ludwieg tubes. This effect was tested in the AFRL Ludwieg tube by allowing up to fifteen minutes for gas motion to damp between the end of driver-tube fill and the beginning of a run. Settling time had no measureable effect on Pitot pressure fluctuations in the AFRL Ludwieg tube. This result emphasizes the dominance of nozzle acoustic radiation on Pitot pressure fluctuations in non-quiet wind tunnels.

Figure 12 illustrates the test section Mach number, measured at the nozzle exit. These Mach numbers were derived from measured Pitot and contraction pressures. Pitot 3, which was the one mounted in a probe rather than probeless configuration, registered a slightly higher Mach number. It is unclear if this difference was due to the transducer or the method of mounting. Figure 12 demonstrates that Mach number was uniform to within +/-1% five inches to either side of centerline.

The Mach number at the nozzle exit was estimated for a variety of stagnation pressures using all combinations of driver tube transducer D, contraction, nozzle exit pressure and Pitot probes. These calculations were performed for fast-valve, single and double diaphragm actuation. The average Mach number for these runs was 6.0, with 2.3% standard deviation. This variation in Mach number was due largely to some outlier pressure transducers, and represents a conservative estimate of the Mach number uncertainty. The actual uncertainty in Mach number is probably much less, and should improve with better calibration procedures. There was no observable trend between Mach numbers measured between the first and second periods of steady flow.

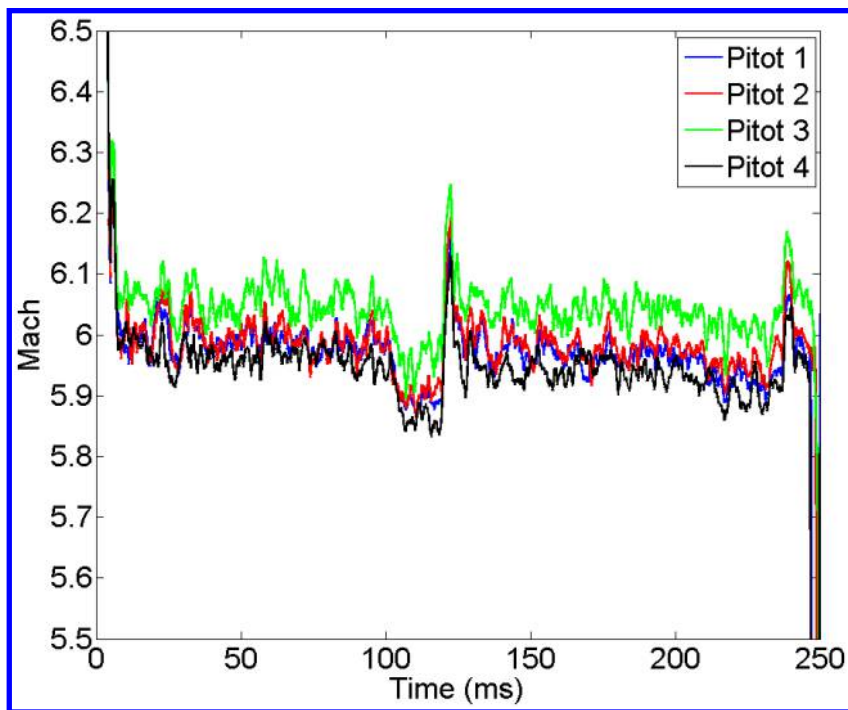
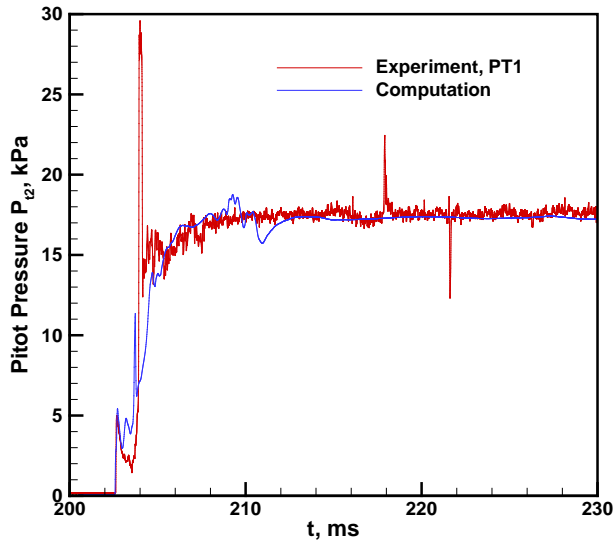


Figure 12 Mach number

#### F. Tunnel Start Calculations and High-Speed Schlieren

Tunnel pressures measured during a diaphragm-actuated test were compared to computations and high-speed schlieren images to better understand the startup process. Figure 13 compares measured and computed Pitot pressures at the nozzle exit. These pressures were calculated using the EILMER3 code<sup>10,11</sup> using an axisymmetric grid. This test was actuated by a single diaphragm, with a stagnation pressure of 100 psia. The single diaphragm case was chosen since it was the most straightforward to simulate. The computed pressures were time-shifted so that the initial pressure rise from the starting shock was coincident with the measured rise. Although the timing and amplitude of pressure features varied slightly between the computation and experiment, the computation captured the essential features of the starting process.



**Figure 13 Comparison of computed to measured Pitot pressure during tunnel start**

High-speed schlieren images obtained during the same run, shown in Figure 14, show flow events correlated with the Figure 13 pressure traces. Figure 14 shows the Pitot rake oriented in the horizontal plane. The initial pressure spike at  $t=202.6$  ms results from the shock from the diaphragm opening, as it passes over the probe. Flow behind the bow shock is subsonic, and the starting shock reflects upstream, as illustrated by image 3 of Figure 14. Flow goes supersonic over the probe in image 4, at 203.9 ms, followed by another wave passage. These events are correlated with a second spike in Pitot pressure. The flow continues to develop until about  $t=212.6$  ms. After this time, the flow remains quasi-steady. Pitot pressure also plateaus at this time, with the exception of transient noise, including some spikes due to particle passage. Further images and analysis of the tunnel start process, along with details of the schlieren system are given in a companion paper.<sup>12</sup>

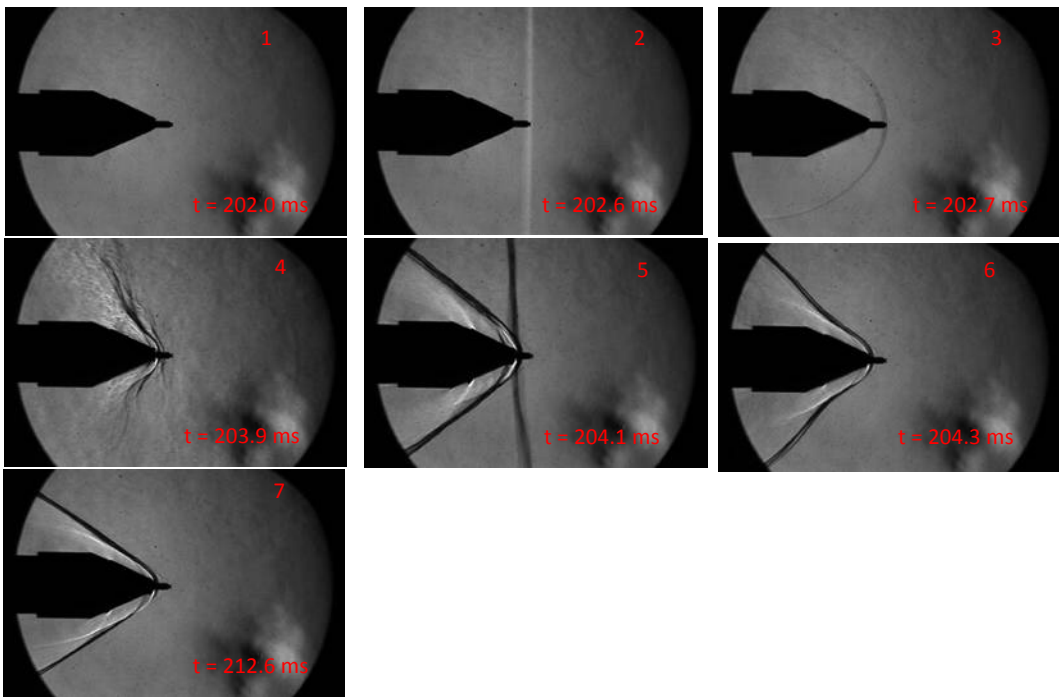
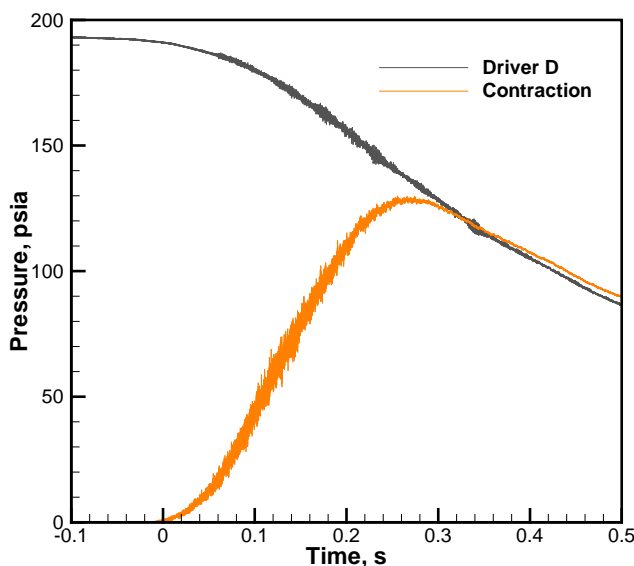


**Figure 14 Schlieren images of Pitot rake during single-diaphragm startup**

### G. Ball Valve Performance

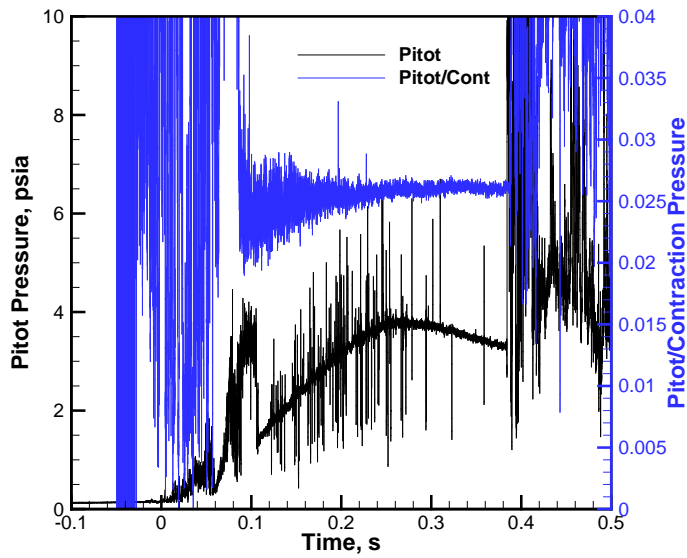
A 10 inch diameter, quick-opening ball valve was acquired during the construction of the wind tunnel to isolate diaphragms and the fast valve from the driver tube. The measured opening time for this valve was 1.1 s. Although the valve would not be fully open at the time the tunnel started (and in fact would continue opening throughout the test run), it was estimated that the valve actuation would be fast enough to start the wind tunnel and provide some period of hypersonic flow. Since the valve opening time is longer than the time required for expansion waves to propagate to the end of the driver tube and back, the stagnation pressure during a ball valve test would not show periods of steady reservoir conditions (as it does for the diaphragms and fast-valve), but would instead show a continuous drop during the run. Nevertheless, there might be situations where this would not be objectionable. Therefore, several tests were carried out using the ball-valve alone for actuation.

Tests showed that the tunnel did not fully start using the ball valve for initial driver pressures of 100 psi or less. The ball valve did start, however, for higher pressures. Figure 15 shows the driver tube D pressure and contraction pressure for a ball valve run with initial driver pressure of 200 psi. As expected, the driver tube pressure drops continuously during the run, not in a stepwise fashion as it did when the tunnel was actuated with diaphragms or fast valve. The contraction pressure takes about 280 ms to rise from its pre-run vacuum pressure to a level approaching the driver tube pressure. After this time, it drops continuously in concert with the driver tube pressure.



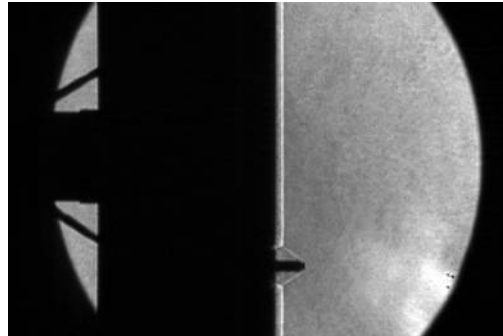
**Figure 15** Driver tube and contraction pressures during 200 psi ball valve run.

Figure 16 shows Pitot pressure measured during the same 200 psi ball valve test. The Pitot pressure shows numerous spikes. Based on schlieren data, these are attributed to particle impacts that occurred during the test. The Pitot pressure history was similar to the contraction pressure history, rising to a maximum at about 280 ms, and dropping after that. Unstart occurred at about 380 ms. Despite the unsteady conditions, the normalized Pitot pressure,  $pt_2$ , divided by the contraction pressure, is constant at 0.027 between 280 and 380 ms. This Pitot pressure ratio indicates a Mach number of 6.1 in the test section.



**Figure 16 Pitot pressure during 200 psi ball valve run, dimensional and normalized.**

The schlieren image of the Pitot rake during a 200-psia stagnation pressure ball valve test is shown in Figure 17. The Pitot rake in this case was rotated to lie in the vertical plane. The bow shock is stable and well-formed, demonstrating supersonic flow.



**Figure 17 Schlieren image of Pitot rake during 200 psi ball-valve run**

#### H. Comparative Noise Characteristics

Figure 18 shows measured RMS Pitot pressure fluctuations as a function of the initial driver pressure. With the exception of the ball valve data, these data are based on Pitot pressures measured during the first period of quasi-steady flow. The ball valve RMS data were obtained in the period between the initial maximum Pitot pressure and unstart. There was no discernible trend in noise levels between the first and second periods of quasi-steady flow. Generally, single diaphragm actuation provide slightly lower noise levels than double diaphragm actuation. This is probably due to cleaner breakage of the single-diaphragm runs. The red symbols in Figure 18 were obtained from single and double diaphragm runs in which one or more petals of the diaphragm failed to fully open. Fluctuation levels from these partially-obstructed runs were generally higher than for runs with clean diaphragm breakage. The fast valve fluctuation levels are somewhat higher than for a clean diaphragm break, but are still reasonable for a conventional wind tunnel. The highest fluctuation levels occur during the ball valve runs, presumably due to the obstruction created by the partially open ball valve.

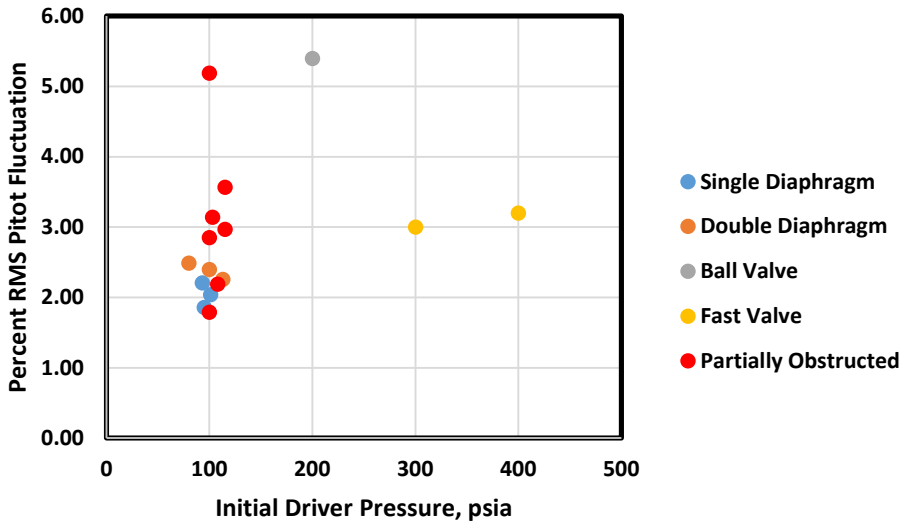


**Figure 18 Pitot pressure fluctuations**

## V. Conclusions and On-Going Work

The AFRL Ludwieg tube has been demonstrated to provide well-defined Mach 6 flow. The tunnel performs to specifications, and with a fast-valve can be operated about every five minutes at driver pressures up to 200 psi. Tunnel operation has been demonstrated using Mylar® diaphragms, single and double metal diaphragms, a fast valve and a ball-valve. Tunnel noise characteristics have not been fully quantified, but appear similar to other large conventional wind tunnels. Obstructions in the driver tube due to partial diaphragm breaks or partially-opened valves are associated with higher noise levels.

Additional work is underway to enhance tunnel operation and characterize the flow still further. A larger rake has been fabricated with provision for Kulite and PCB® transducer Pitot probes. This rig will be used to map out the spatial and temporal flow uniformity in more detail. Boundary-layer transition measurements will provide additional assessment of the tunnel flow fluctuations.

## Acknowledgments

Numerous staff of the University of Dayton Research Institute assisted in the tunnel design and construction, including William Braisted, Michael Frede, Rebecca Hoffman, Kevin Roach, Jesse Thumser and Keith Vehorn. Christopher Huffman of Notre Dame assisted with data analysis. The fast valve was supplied by HST, GmbH. Michael Semper of the Air Force Academy, John Schmissuir (AFOSR and University of Tennessee Space Institute), Steven Schneider (Purdue University), and Lawrence Leny (AFRL) provided valuable support and information.

## References

- <sup>1</sup> Friehmelt, H., Koppenwallner, G., and Müller-Eigner, R., "Calibration and First Results of a Redesigned Ludwieg Expansion Tube," AIAA Paper 93-5001.
- <sup>2</sup> Wolf, T., Estorf, M., Radespiel, R., "Investigation of the starting process in a Ludwieg tube," *Theoretical and Computational Fluid Dynamics*, vol 21, 2007, pp. 81-98.
- <sup>3</sup> Schrijer, F. F. J. and Bannink, W. J., "Description and Flow Assessment of the Delft Hypersonic Ludwieg Tube," AIAA paper 2008-3943, June 2008.
- <sup>4</sup> Juhany, K. A., and Aldakhil, H., "AT0 Ludwieg Tube Wind Tunnel at KAU," AIAA paper 2006-1316, January 2006.

<sup>5</sup> Decker, R. K., Semper, M. T., Anthony, J. D. and Cummings, R. M., “Starting Characteristics of the US Air Force Academy Mach 6 Ludwieg Tube,” AIAA paper 2015-3338, June 2015.

<sup>6</sup> Keener, E. R. and Hopkins, E. J., “Accuracy of Pitot-Pressure Rakes for Turbulent Boundary-Layer Measurements in Supersonic Flow,” NASA TN D-6229, March 1971.

<sup>7</sup> Cummings, R. M., and McLaughlin, T. E., “Hypersonic Ludwieg Tube Design and Future Usage at the US Air Force Academy,” AIAA paper 2012-0734, January 2012.

<sup>8</sup> Knauss, H., Riedel, R., and Wagner, S., “The Shock Wind Tunnel of Stuttgart University – a Facility for Testing Hypersonic Vehicles,” AIAA paper 1999-4959, 1999.

<sup>9</sup> Liepmann, H. W. and Roshko, A., *Elements of Gasdynamics*, Galcit Aeronautical Series, John Wiley & Sons, Inc., New York, 1957, p75.

<sup>10</sup> Gollan, R.J. and Jacobs, P.A. (2013), “About the formulation, verification and validation of the hypersonic flow solver Eilmer,” *International Journal for Numerical Methods in Fluids* 73:19-57 (DOI: 10.1002/fld.3790)

<sup>11</sup> Chan W.Y.K., Jacobs P.A, and Mee D.J. (2011, “Suitability of the k-omega turbulence model for scramjet flowfield simulations,” *International Journal for Numerical Methods in Fluids*, vol. 70, no. 4, pages 493-514 (DOI: 10.1002/fld.2699)

<sup>12</sup> Lam, K.-Y., Pickles, J. D., Narayanaswamy, V., Carter, C. and Kimmel, R., “High-Speed Schlieren and 10-Hz Kr PLIF for the new AFRL Mach-6 Ludwieg Tube Hypersonic Wind Tunnel,” submitted to AIAA Scitech 2017.